Effect of Sequence Length, Sequence Frequency, and Data Acquisition Rate on the Performance of a Hadamard Transform Time-of-Flight Mass Spectrometer

Facundo M. Fernández, José M. Vadillo, Friedrich Engelke,*
Joel R. Kimmel, and Richard N. Zare
Department of Chemistry, Stanford University, Stanford, California, USA

Nestor Rodriguez
Molecular Structure and Dynamics, ESML, Pacific Northwest National Laboratory, Richland, Washington, USA

Magnus Wetterhall and Karin Markides
Department of Chemistry, Uppsala University, Uppsala, Sweden

Various factors influencing the performance of a Hadamard transform time-of-flight mass spectrometer (HT-TOFMS) have been investigated. Using a nitrogen corona discharge to produce an ion stream of N_2^+, N_3^+, and N_4^+, it is found for spectra containing only N_4^+ that the signal-to-noise ratio (SNR) closely approaches the value calculated from the ion background by assuming that the ion background follows a Poisson distribution. In contrast, for a more intense beam containing N_2^+, N_3^+, and N_4^+, the SNR is less than its theoretical value because of the appearance of discrete spikes in the mass spectrum caused by deviations in the actual modulation sequence from the ideal one. These spikes can be reduced, however, by decreasing the modulation voltage. Under these optimized conditions, the pseudo-random sequence length is varied to understand how it alters SNR, mass resolution, and scan speed. When the length of the pseudo-random sequence is doubled, the SNR increases by $\sqrt{2}$ while the time necessary to record a mass spectrum also doubles. Mass resolution can be varied between 500 and 1200 at $m/z = 609$ as the sequence length, modulation speed (10 MHz, 25 MHz), and acquisition rate (up to 50 MHz) are changed. Scan speeds of 6000 passes per s can be obtained using a sequence containing 4095 elements modulated at 25 MHz. The capability to tailor the HT-TOFMS to increase the scan speed and resolution with a constant 50% duty cycle makes the technique extremely appealing as a mass analyzer for measuring rapid changes in the composition of an ion stream. (J Am Soc Mass Spectrom 2001, 12, 1302–1311) © 2001 American Society for Mass Spectrometry

Time-of-flight mass spectrometry (TOFMS) requires measurements of the differences in arrival times of ions to the detector [1]. The intrinsic time difference nature of TOFMS makes it a natural choice for pulsed ion sources, such as matrix-assisted laser desorption ionization [2, 3] (MALDI). For continuous ion sources, however, the use of TOFMS faces the challenge of overcoming the loss of ions during the mass analysis cycle. Typically, TOFMS is operated in a manner such that an ion packet cannot be injected into the drift region until the slowest ion for the packet preceding it has reached the detector. One possible way to circumvent this problem is to use ion traps [4]. Ions exiting the source are stored in the ion trap, extracted by a short pulse (gate), and finally accelerated toward the drift region. Another scheme involves the use of a slow ion beam and orthogonal extraction into the drift region of a time-of-flight instrument [5].

Brock, Rodriguez, and Zare [6, 7] have proposed and implemented a radically different approach that achieved a 50% duty cycle without sacrificing the advantages of TOFMS in terms of low cost and the ability to detect all mass peaks at the same time. This method consists of on-axis modulation of the incoming ions by means of a well defined pseudo-random sequence of pulses that transmits or deflects the ion

Published online October 23, 2001

Address reprint requests to Dr. R. N. Zare, Department of Chemistry, Stanford University, Standford, CA 94305-5080, USA. E-mail: zare@stanford.edu

*Currently at Fachhochschule Furtwangen, University of Applied Sciences, Villingen-Schwenningen, Germany.

1044-0305/01/$20.00
PII S1044-0305(01)00322-1

Received July 9, 2001
Revised August 30, 2001
Accepted August 30, 2001

stream. In this sense, the ion beam produced in the ionization region is itself chopped into discrete ion packets of different lengths. The ions in these packets travel through the flight tube at different velocities, with typical flight times of hundreds of microseconds. At the point of modulation, the temporal width of the ion packets and the time between adjacent packets is three orders of magnitude shorter than these flight times. As the packets travel the length of the flight tube, ions of different mass/velocity become spatially resolved, causing adjacent packets to overlap. The output signal corresponds to the convolution of many conventional TOF mass spectra shifted in time following the modulation sequence. To extract a TOF mass spectrum from this data, the signal is demodulated using knowledge of the applied pseudo-random sequence. The demodulation corresponds mathematically to an inverse Hadamard transform [8]. The Hadamard transform belongs to the same family of transforms as the Fourier transform. In the Fourier transform, the basis functions used to decompose the time domain signal are an infinite series of sines and cosines. In the Hadamard transform, we deal with a finite series of binary elements known as Walsh functions. The Hadamard transform provides several advantages over the Fourier transform: It is about ten times faster to compute, it does not have aliasing effects, and it is applicable to situations where a series of on and off phenomena are recorded [9] and it has been successfully applied to other problems in chemistry such as Raman imaging [10, 11]. As the technique makes use of this mathematical deconvolution, the name Hadamard transform time-of-flight mass spectrometry (HT-TOFMS) has been coined to describe it.

The theoretical background and experimental results presented in this work demonstrate the unique capabilities of HT-TOFMS. The influence of the length and frequency of the pseudo-random sequence and signal acquisition rate on figures of merit such as scan speed, mass range, and resolution have been evaluated. Results using a nitrogen corona discharge and an electrospray source, both of which are continuous ion sources, are presented and discussed.

Experimental

Reagents

The solvent for all electrospray experiments was a 50:50 vol/vol mixture of high purity water (18 MΩcm^{-1}) and methyl alcohol (Aldrich Chemical Co., St. Louis, MO) with 0.001 M acetic acid (Aldrich) added. Reserpine (11,17-dimethoxy-18-[{3,4,5-trimethoxybenzoyl}oxy]-methyl ester[3β,16β,17α,18β,20α]-[9Cl], Aldrich) was used without further purification. A poly(propylene glycol) standard (Scientific Polymer Products Inc., Ontario, NY) with an average molecular weight of 450 aμ was used for mass calibration purposes.

HT-TOF Mass Spectrometer

In corona discharge experiments, the basic configuration of the HT-TOF mass spectrometer, the modulation signal generator, and the data acquisition system were identical to those described previously [6, 7]. The spectra were collected operating in gate mode [7]. In this mode, no shifts in peak positions are observed.

In electrospray ionization (ESI) experiments, the ion optics scheme was changed from the original quadrupole–octopole configuration. A single octopole was used to guide the ions from the first pumping stage to the Einzel lenses before the grid modulator. Details about the new ion guide and the ESI interface are given below.

Corona Discharge Experiments

The corona discharge experiments were performed by applying 600 V between the transfer capillary and the first stage skimmer (typically spaced 5 mm apart). The ionization gas was supplied by connecting an electrically isolated nitrogen gas line to the transfer capillary. In order to obtain a stable and intense discharge the nitrogen flow rate was regulated by a metering valve. In addition, a 10 MΩ / 2W resistor was connected in series with the transfer capillary to limit the ion current and further stabilize the discharge. The typical pressure inside the discharge chamber was 0.3 torr.

Electrospray Ionization Source

The electrospray ion source was modified from the one described in previous work [7]. Sheathless electrospray emitters were constructed following the procedure described by Barnidge et al. [12]. Briefly, the tip of a 25 μm i.d. x 360 μm o.d. fused silica capillary (Polymicro Technologies, Tucson, AZ) was first mechanically sharpened. Electrical contact between the tip and the flowing liquid was provided by Au particles (2 μm diameter, Aldrich) glued to the tip of the capillary with polyimide sealing resin (Supelco). During the coating process, the capillary was constantly purged with N_2 to avoid clogging. The polyimide resin was cured overnight at 200 °C.

During electrospray operation, solutions were nebulized with a syringe pump (Harvard Apparatus, Southnatick, MA) fitted with a 250 μL syringe (Hamilton, Reno, NV). The solutions were pumped at a flow rate of 500 nL min^{-1}. Typically, 2100 V were applied to the emitter tip that was mounted in an XYZ micro-positioning stage facing the grounded counter plate (Figure 1, bottom). The design of this plate was critical for maximizing sensitivity. The counter plate consists of a circular piece of bronze with a centered conical inlet (1.3 cm o.d) and a piece of stainless steel tubing (1.6 mm o.d., 250 μm i.d., 15 mm long) inserted through it. This counter electrode was mounted on the first differentially pumped region of the mass spectrometer (operat-

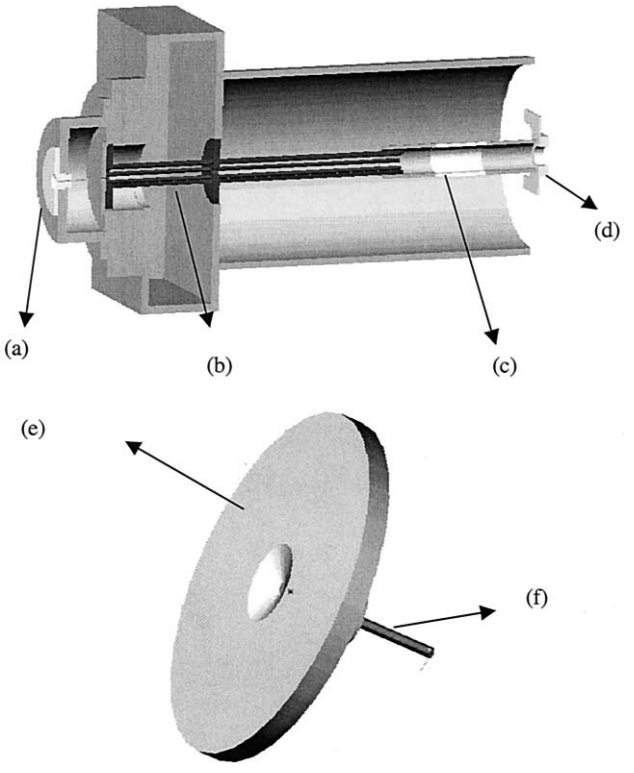

Figure 1. Schematic of the HT-TOFMS spectrometer. Top: first three differentially pumped regions of the instrument: (**a**) Interface, (**b**) octopole, (**c**) cylindrical lenses, (**d**) ion beam modulator. Bottom: Electrospray interface, (**e**) ground plate, (f) nozzle.

ing at 2.7 torr and 110 °C). After optimizing the position of the tip, the intensity of the signal varied by no more than 6% over a 30 min period.

The following region, extending from the skimmer to the middle of the octopole, was held at 10^{-2} torr to assist in solvent removal (Figure 1, top). After passing through a third pumping region (5×10^{-5} torr) that includes the second half of the octopole, the Einzel lenses, and the ion beam modulator, ions enter the flight tube (3×10^{-6} torr). A restrictor (3 mm diameter) placed between the third stage and the flight chamber ensures a steady pressure in it and prevents condensation on the detector surface.

Octopole Ion Guide

Ions from the ESI source were extracted using a 238 mm long octopole ion guide (Figure 1, top). The octopole is made from 3.175 mm diameter stainless steel rods (AISI 316) with an open clearance between rods of 14 mm. The octopole was driven by a radio frequency power supply (model 011 with Q-head no.15, Extranuclear Laboratories, Pittsburg, PA) set to a frequency of 2.5 MHz in RF-only mode. The radio frequency amplitude is adjusted for optimum ion signal and low mass rejection, and is usually ~700 V. This octopole ion guide cools, focuses, and directs the generated ions to the focusing lenses. An octopole was used in place of a quadrupole because of the superior transmission properties [13]. Octopoles ion guides have a wider and deeper effective potential than quadrupoles and hexapoles. This allows transporting more ions to the focusing lenses with less space charge effects, resulting in improved resolution and sensitivity. Because our modulation grid has a large active area (25 mm^2), the increased beam diameter does not affect resolution. Owing to collisional cooling, ions traversing the octopolar ion guide lose energy, thus resulting in an ion beam with less energy spread both in the radial and longitudinal directions [14].

Sequence Generator and Ion Modulator

Hadamard sequences used to modulate the ion beam are known as maximum length pseudo-random sequences [8]. The different pseudo-random sequences were generated with the sequence generator described previously [7]. The only modifications required were those needed to modify the sequence length, which involved changing the connections between outputs of the shift registers and the XOR gate in charge of computing the sequence. A detailed circuit diagram and a discussion of its operational principles can be found in our previously cited article. These sequences have lengths $N = 2^b - 1$, where b is the number of bits in the sequence. Typical values of N are 2047 for $b = 11$, 4095 for $b = 12$, and 8191 for $b = 3$. As an example, an 11-bit sequence is obtained when bits 9 and 11 from the shift registry chain are fed to the XOR gate. Experiments to determine the effect of sequence length on scan speed, mass range, and signal-to-noise ratio were carried out using sequences of 11, 12, and 13 bits. In all of these cases, the duty cycle is 50%, because all the sequences used have approximately equal numbers of 0's and 1's.

The output of the pseudo-random sequence generator was split into two phases of opposite polarity; each phase was amplified independently and added to the liner voltage of the flight chamber (−1250 V) that is also used to float the ion modulator frame. The resultant signals were applied to the two isolated wire sets of a charged particle modulator (CPM) based on the interleaved comb ion deflection gate described by Vlasak et al. [15]. When the logical output of the sequencer is 1, and the modulation voltage is set to 15 V, the positive set of wires in this modulator has an average voltage of −1235 V (liner plus phase I) and the negative set of wires has an average voltage of −1265 V (liner plus phase II). In this way, the ions passing through the modulator are deflected and do not reach the detector. When the element in the sequence is a 0, both sets of wires have the same voltage (−1250 V) and the ions are undeflected.

Theoretical Background

We begin by presenting the mathematical background necessary to understand the advantages that Had-

amard-multiplexed MS provides compared to a dispersive TOFMS. A detailed description of the arguments is beyond the scope of this article. Only the most relevant aspects will be highlighted. The references cited in this section provide extensive information on this topic.

Let us assume that we want to record one mass spectrum that is characterized by a set of N parameters $\{\Psi_1, \Psi_2, \ldots, \Psi_N\}$ representing the abundance of each ion species reaching the detector at different flight times in an ideally noiseless situation. In any measurement, the signal intensity for each ion, Ψ_i, will have an associated uncertainty u_i; therefore, the experimental value of Ψ_i in the measured mass spectrum is given by z_i:

$$z_i = \Psi_i + u_i \tag{1}$$

The values Ψ_i can be measured using either a dispersive (conventional) method or a multiplexing method.

Conventional Method

The conventional method involves collecting the signal for a given time period spanning the flight times of the lightest and the heaviest ions in increments Δt. Each Ψ_i is measured individually as follows:

$$\begin{aligned} z_1(t_0) &= a_1\Psi_1 + u_1 \\ z_2(t_0 + \Delta t) &= a_2\Psi_2 + u_2 \\ &\vdots \\ z_N(t_0 + (N-1)\Delta t) &= a_N\Psi_N + u_N \end{aligned} \tag{2}$$

where a_i is always 1, because the relative weight of every measurement is identical. This set of equations can be expressed in matrix form by

$$Z = (I \cdot \Psi) + U \tag{3}$$

where U is the column vector whose coefficients, u_i, are the errors (noise) associated with each measurement and I is the identity matrix. Operating under detector-noise-limited conditions, the noise is sampled with the same weight as Ψ_i. Under the conventional method, the SNR for Ψ_i, $\mathrm{SNR}_{\mathrm{conv},i}$, is given by the well-known expression

$$\mathrm{SNR}_{\mathrm{conv,i}} = \frac{\Psi_i}{\sigma_{\mathrm{conv}}} \tag{4}$$

where σ_{conv} is the standard deviation of the measurement. To improve $\mathrm{SNR}_{\mathrm{conv},i}$ data must be collected for extended periods of time. In many situations increasing the sampling time is not possible. Consider for example the analysis of unique single events such as individual laser shots or the very narrow transient signals obtained in flow-injection analysis, gas chromatography, and electrophoretic separations.

Multiplexing Method

Multiplexing involves the simultaneous measurement of different combinations of ions reaching the detector. The signal at a time t_N, defined as z_N, is then a weighted sum of the original variables Ψ_i. The magnitude of the weighting factors, a_i, varies with time:

$$\begin{aligned} z_1(t_0) &= a_{11}\Psi_1 + a_{12}\Psi_2 + \ldots + a_{1N}\Psi_N + u_1 \\ z_2(t_0 + \Delta t) &= a_{21}\Psi_1 - a_{22}\Psi_2 + \cdots - a_{2N}\Psi_N + u_2 \\ &\vdots \\ z_N(t_0 + (N-1)\Delta t) &= a_{N1}\Psi_1 + a_{N2}\Psi_2 + \cdots + a_{NN}\Psi_N + u_N \end{aligned} \tag{5}$$

This set of equations can be expressed in a matrix form:

$$Z = (H \cdot \Psi) + U \tag{6}$$

where H is the matrix containing of all the coefficients a_i for each Ψ_I and U is the non-modulated background noise. For example, for a set of four variables $\{\Psi_1, \Psi_2, \ldots, \Psi_N\}$, H is a 4 by 4 matrix:

$$H_4 = \begin{bmatrix} a_{11} & a_{12} & a_{13} & a_{14} \\ a_{21} & a_{22} & a_{23} & a_{24} \\ a_{31} & a_{32} & a_{33} & a_{34} \\ a_{41} & a_{42} & a_{43} & a_{44} \end{bmatrix} \tag{7}$$

For the purpose of multiplexing, a very efficient weighting design [16] is obtained using Hadamard matrixes:

$$H_4 = \begin{bmatrix} 1 & 1 & 1 & 1 \\ 1 & -1 & -1 & 1 \\ 1 & 1 & -1 & -1 \\ 1 & -1 & 1 & -1 \end{bmatrix} \tag{8}$$

The coefficients a_i are chosen to be 1 for the first column and row, and combinations of $+1$ and -1 are chosen for the other elements. In Hadamard matrixes, the rows are linearly independent; hence the scalar product of any two rows is zero.

If a multiplexing experiment is performed using the Hadamard matrix H as the basis for the weighting design, the values Ψ_i can be found using the inverse of the Hadamard matrix, H^{-1}:

$$\Psi = H^{-1} \cdot (Z - U) \tag{9}$$

Solving this expression would require measuring the noise U, calculating $H^{-1}\cdot U$ and then subtracting this quantity from $H^{-1}\cdot Z$. For statistically distributed noise, this inverse Hadamard transform distributes the noise evenly over all the measurements. Hence the contribution of $H^{-1}\cdot U$ to Ψ is negligible for $N \gg 1$, and there is no need to measure the background separately. This feature is an important characteristic of the use of Hadamard transforms.

For the HT method, the standard deviation σ_H of the parameter Ψ_i is given by [8]:

$$\sigma_{\mathrm{H,i}} = \frac{\sigma_{\mathrm{conv,i}}}{\sqrt{N}} \tag{10}$$

and the signal-to-noise ratio $\mathrm{SNR_{H,i}}$ is:

$$\mathrm{SNR_{H,i}} = \frac{\Psi_{\mathrm{i}}\sqrt{N}}{\sigma_{\mathrm{conv,i}}} = \sqrt{N}\,\mathrm{SNR_{conv,i}} \tag{11}$$

Hadamard matrices make the best weighting designs when the weight factors are -1 or $+1$. In our mass spectrometer, the ion beam is modulated on and off. Such a binary situation requires the weighting factors to be 1 (deflected beam) or 0 (undeflected beam). To accommodate this experimental situation, a scheme called a Simplex design is derived from the Hadamard matrix. The resulting Simplex matrix, S_N, is obtained by removing the first row and the first column of the matrix H_{N+1} and replacing the remaining $+1$'s with 0's and the remaining -1's with $+1$'s. The matrix $\mathrm{H_4}$ defined above leads to the matrix S_3:

$$S_3 = \begin{bmatrix} 1 & 1 & 0 \\ 0 & 1 & 1 \\ 1 & 0 & 1 \end{bmatrix} \tag{12}$$

It can be shown [8] that the signal-to-noise ratio in a Simplex experiment, $\mathrm{SNR_S}$, is:

$$\mathrm{SNR_{S,i}} = \frac{N+1}{2\sqrt{N}}\,\mathrm{SNR_{conv,i}} \approx \frac{\sqrt{N}}{2}\,\mathrm{SNR_{conv,i}} = \frac{1}{2}\,\mathrm{SNR_{H,i}} \tag{13}$$

Simplex matrices can be generated by several means. In this work, simplex matrices are developed using maximum length pseudo-random sequences. The first row of any S-matrix is a pseudo-random sequence. Shifting this row by one element creates the second row of the cyclic S-matrix. Shifting N times gives S_N. A unique property of pseudo-random sequences is that they minimize the error in the deconvoluted spectra [17]. It is for that reason they were chosen in our experiment.

Comparison of the theoretical SNR using Hadamard multiplexing, Simplex multiplexing, and conventional detection predicts a significant improvement occurs through multiplexing. This improvement is referred to in the literature as the Fellgett advantage, G_{M}. For the case of intensity-independent detector noise, the Hadamard and Simplex multiplexing gains, $G_{\mathrm{M,H}}$ and $G_{\mathrm{M,S}}$ are:

$$G_{\mathrm{M,H}} = \frac{\mathrm{SNR_H}}{\mathrm{SNR_{conv}}} = \sqrt{N} \tag{14}$$

and

$$G_{\mathrm{M,S}} = \frac{\mathrm{SNR_S}}{\mathrm{SNR_{conv}}} = \frac{N+1}{2\sqrt{N}} \approx \frac{\sqrt{N}}{2} \tag{15}$$

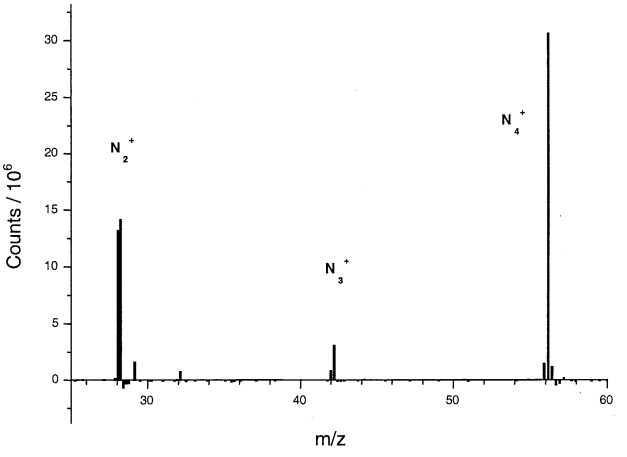

Figure 2. HT-TOF mass spectrum of a N_2 corona discharge.

As an example of this gain, consider a 13-bit pseudo-random sequence. The total number of states is $N = 8191$. Thus, the theoretical multiplexing gains are $G_{\mathrm{M,H}} \cong 90$ and $G_{\mathrm{M,S}} \cong 45$. Many spectrometers operate with additional sources of noise, such as shot noise and flicker noise. In their analysis, Harwit and Sloane [8] concluded that under shot-noise-limited conditions, Hadamard transform spectroscopy did not have a multiplexing advantage. In sharp contrast, Wilhelmi and Gompf [17] developed a detailed theory for neutron beams modulated with a pseudo-random sequence. They found that even under shot-noise-limited conditions a multiplexing advantage is obtained. This advantage is present for $N \gg 1$ and for a sparse spectrum consisting of a few strong lines. When the spectrum is not sparse, the gain in signal-to-noise ratio decreases, but, as noise increases, it tends asymptotically to the value predicted by Harwit et al. [8]. In our experiments, the signal-to-noise ratio gain we obtained was in accordance with the expected theoretical values from Wilhelmi and Gompf [17].

Results and Discussion

Sources of error in HT-TOFMS

Understanding the different sources of noise that affect the measurements in HT-TOFMS is crucial for understanding the effect of pseudo-random sequences of different length. The main contribution to the baseline noise is the background noise produced by the variance in the total ion signal, which is expected to obey a Poisson distribution. In such a case, the baseline noise should equal the square root of the modulated signal $\sqrt{\Psi}$ [17].

To test this assumption, a simple ion beam was convoluted with a Hadamard sequence. A corona discharge was chosen as it provides a stable and intense ion source. As shown in Figure 2, three main peaks dominate the mass spectra of the ionized gas: N_2^+ (m/z = 28), N_3^+ (m/z = 42), and N_4^+ (m/z = 56).

The simplest spectrum is that of a monomolecular

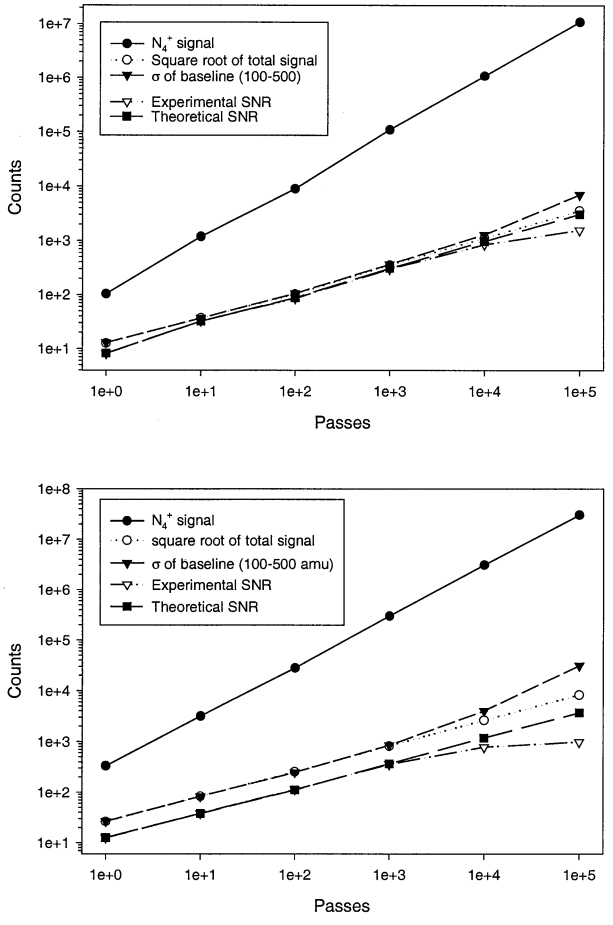

Figure 3. Simplex signal-to-noise ratio SNR_S in a nitrogen corona discharge. (**a**) SNR for a monomolecular ion beam of N_4^+ and (**b**) an ion beam with all nitrogen ionic species.

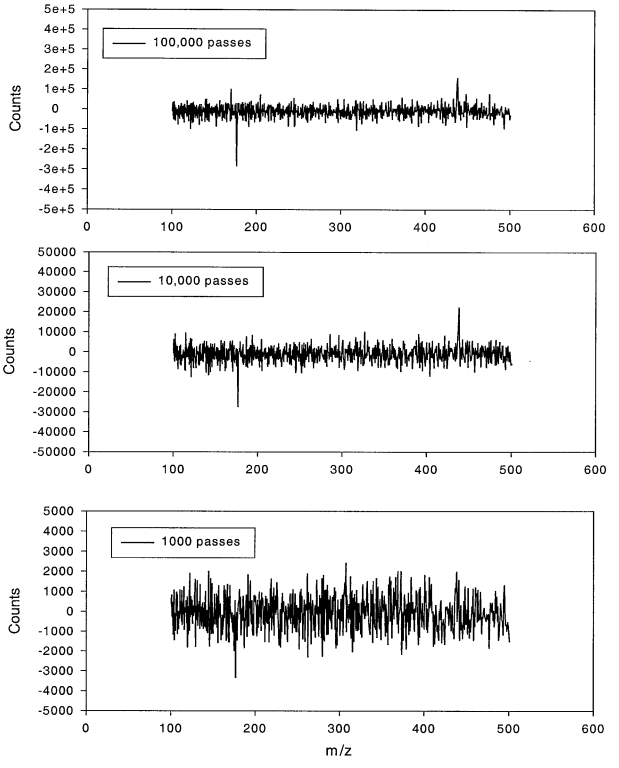

Figure 4. Baseline signal between 100 and 500 aμ for three different acquisition times. One thousand passes correspond to 0.8191 s. The data was acquired in HT-TOFMS mode for a sequence length of 8191 (13 bits) with a modulation voltage of 30 V.

ion beam. In this case the total signal, Ψ, is the sum of the peak signal and the small background noise present in the baseline. Figure 3a shows the SNR_S values when N_4^+ is exclusively present. The experimental value of the SNR_S was calculated by taking the noise as the standard deviation of the baseline in the interval between *m/z* values 100 and 500. The theoretical value was calculated by taking the noise as $\sqrt{\Psi}$. The general trend is that SNR_S increases proportionally to the square root of the number of passes, as expected. In addition, the SNR_S experimental values are in good agreement with the predicted values. When a large number of passes are summed, however, we observed slight deviations from the theoretical SNR. In order to investigate this effect, the octopole ion guide was set so as to transmit all ionic nitrogen species generated in the source, producing a more complex and intense spectrum.

Figure 3b shows the results when the three species observed in Figure 2 significantly contributed to the total signal, Ψ, in the mass spectrum. If the number of passes is kept below 1000, the SNR_S experimental values are again in good agreement with the theoretical predictions. In contrast, if a larger number of passes is summed, the deviation from the theoretical data becomes significant. This effect can be understood by examining the baseline of the TOF spectra when different numbers of passes are summed (Figure 4). It can be clearly seen that some discrete spikes are superimposed onto the background. For a small number of passes (1000) these artifacts are masked as statistical noise. For a larger number of passes (10,000 to 100,000), the intensity of the artifacts increases. As these spikes are not statistically distributed, the baseline variance deviates from the predicted value and thus the experimental SNR_S is smaller than expected. It was also noticed that the intensity of these spikes not only increases with an increase in signal intensity but also with increasing amplitude in the modulation voltage.

The origin of these spikes has been recently modeled for optical spectroscopy by Hanley [19]. Similar considerations are valid for mass spectrometry. When a logical 1 is applied to the ion beam modulator, there is a finite rise time in the voltage output caused by a slight mismatch in the impedances of the modulation grid and the driving electronics. This mismatch results in a trapezoidal pulse instead of a square pulse (also known as Tai type mask defects [19]). Because the *S* matrix used to modulate the signal is slightly different from the *S* matrix used to deconvolute the data, discrete spikes appear as echoes of the main peaks. The intensities of the spikes are a fixed fraction of the intensities

of the main peaks. This fact explains the increased deviations from the theoretical values of SNR_S when the ion beam is more intense, as in Figure 3b. The intensities of the spikes are also a function of the modulation voltage, because the rise times are increased when voltages higher than 20 V are applied. In following ESI experiments the modulation voltage was maintained at 15 V to essentially eliminate echoes without losing significant modulation efficiency.

Effect of Modulation Sequence Length on Signal-to-Noise Ratio

In this set of experiments, our interest was centered on determining the behavior of SNR_S when the length of the pseudo-random sequence was changed. Increasing the number of elements in the sequence (increasing the number of bits) implies increasing its period and thus the number of logical 1's applied to the modulator (that is, the number of on states). The effect is to increase the signal measured for a fixed number of passes, thus improving the SNR_S.

Let us consider two sequences of different length, 11 and 12 bits, respectively. Under the assumptions verified in the previous section, the SNR_S can be described by the following expressions:

$$SNR_S^{11} = \frac{\Psi_{i,11}}{\sqrt{\Psi_{11}}} \quad (16)$$

and

$$SNR_S^{12} = \frac{\Psi_{i,12}}{\sqrt{\Psi_{12}}} \quad (17)$$

In changing from an 11-bit sequence to a 12-bit sequence, the number of 1's in the sequence is increased from 1024 to 2048 [20]. Thus, the signals obtained under these two conditions are related by:

$$\frac{k_{12}}{k_{11}} \cdot \Psi_{i,11} = \Psi_{i,12} (\text{with } k_{11} = 1024, k_{12} = 2048) \quad (18)$$

Eq 18 is also valid for the case where the 12-bit sequence is changed to a 13-bit sequence ($k_{13} = 4096$) and can also be applied to the total signal Ψ_{11}, Ψ_{12}, and Ψ_{13}. When the length of the sequence is increased by 1 bit, there is a $\sqrt{2}$ increase in SNR because both Ψ_i and Ψ are doubled.

To demonstrate this trend, a 100 μM solution of reserpine (in 50:50 MeOH/H_2O, 1 mM acetic acid) was electrosprayed under constant instrumental conditions with applied sequences of 11, 12, and 13 bits. Figure 5 shows that the prominent MH^+ peak of reserpine occurs at about 131 μs. Clearly, the peak intensity increases as k increases as predicted theoretically (eq 18). The number of on states in the matrix is doubled at each step (1024, 2048, and 4096) and so, an increase in

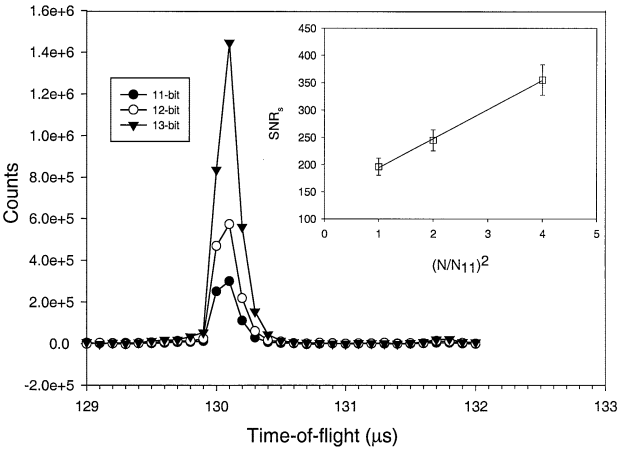

Figure 5. Peak height intensities of a 100 μM solution of reserpine in 50:50 methanol:water (1 mM acetic acid) modulated by different pseudo-random sequences. The insert shows the improvement in SNR as a function of the relative increase in the sequence length compared to a 11-bit sequence (N/N_{11}).

SNR by a factor of $\sqrt{2}$ is produced (Figure 5, insert). Long pseudo-random sequences will have a larger number of 1's and more ions will be monitored. In this sense, the effect is the same as increasing the dwell time of each channel in a scanning spectrometer.

At first sight, it may seem that longer sequences offer unquestionable advantages over shorter ones. But long sequences also have long periods equal to $N \cdot \Delta t$, and thus, the time required to monitor a single pass is doubled when the number of bits is increased by 1. The selection of the length of the pseudo-random sequence used must be determined taking into account not only the SNR_S but also other parameters such as the working mass range, the maximum scan speed, and the mass resolution. In general, longer sequences yield larger mass ranges and higher sensitivity whereas shorter sequences provide higher scan speeds with lower SNR_S values. Table 1 summarizes this behavior.

Effect of Sequence Length and Frequency on Mass Resolution and Mass Range

In TOF mass spectrometry, differences in the arrival time of isomass ions at the detector produce a decrease in resolution. These differences can arise from the finite spatial width of the ion packet within the modulation region of the mass spectrometer. If a cloud of ions of the same mass with significant spatial width is given the same accelerating energy, the ions achieve the same velocity and will strike the detector surface at times that are dictated by their initial starting positions. Each ion experiences a flight-time error that is related to this initial position spread. The finite dimensions of the ion packet being analyzed will limit the time resolution of the TOFMS (for an ideal detector).

This behavior is not the case in HT-TOFMS, where the time resolution is given by one time unit Δt of the pseudo-random sequence (assuming infinitely sharp

Table 1. Resolution, scan speed, and mass range of the HT-TOFMS for different modulation and data sampling conditions

MLPRS length	Time interval of modulation (ns)	Acquisition bin width (ns)	Mass resolution at $m/z = 609$ (50,000 passes)	Maximum number of passes per s	Maximum mass range (KDa)
11	100	100	294	4885	1.5
		50	514	4885	1.5
		20	601	4885	1.5
12	100	100	307	2442	6.0
		50	435	2442	6.0
	40	40	1130	6105	1.0
		20	1105	6105	1.0
13	100	100	415	1220	12.0*
		50	485	1220	12.0*
	40	40	1232	3052	3.8
		20	1203	3052	3.8

*Corresponds to the mass cutoff, see discussion.

rise times for modulation). This time unit determines the spatial length of the ion packet. After the beam is modulated, the sampling of the signal collected at the detector must be done in integer fractions of Δt (the largest allowed sampling bin width is one time unit). Sampling of the signal waveform into bins of integer fractions $1/p$ of Δt requires a corresponding increase in the total number of sampling bins to cover the whole sequence length. This procedure is called over-sampling. The inverse Hadamard transform procedure is set for the one-time-unit interval; therefore, the deconvolution of over-sampled spectra requires that the signal waveform be inversely transformed separately in sets of every second, third, or whatever $(1/p)^{th}$ multiple that was used in increasing the sampling density. After transformation, the individual sets must be reconstructed to form the TOF distribution. Provided that there is a mass calibration, over-sampling will increase the mass accuracy, but only leads to limited improvement in the time or mass resolution. Experimentally, we observed an improvement in mass accuracy for reserpine that is proportional to the acquisition bin width and independent of the modulation bin width, noting that the peak maximum position did not change with the modulation frequency. With an acquisition bin width of 100 ns the mass accuracy is 1537 ppm, at 40 ns it is 615 ppm, at 20 ns it is 307 ppm, and at 5 ns it is 77 ppm. Mass accuracy is not affected by sequence length.

Figure 6 illustrates the effect of different modulation and acquisition frequencies in the mass spectra of electrosprayed reserpine. As observed in Figure 6a, a single peak for reserpine is present when both the modulation and acquisition bins are set at 100 ns. Under these experimental conditions the mass resolution ($m/\Delta m$) of our system is 307. By decreasing the acquisition bin width (Figure 6c) the resolution slightly increased to 435. When the modulation and the acquisition bin were both decreased to 40 ns, a 2.5-fold increase in the resolution (from 307 to 777) was observed (corresponding to the 2.5-fold decrease in the modulation bin width). This resolution increase allows the observation of three isotopomers of reserpine at 609, 610, and 611 aμ. The relative intensities match the expected ratios (100:37.3:8.5) based on ^{13}C content for natural abundance. Maintaining a modulation bin width of 40 ns and decreasing the acquisition bin width to 20 ns yields a better definition of the ion peaks and thus, additional resolution is obtained. The spectrum, showing a resolution of 1105, is presented in Figure 6d. Resolution is unaffected by changes in the length of the pseudo-random sequence, as shown in Table 1.

The maximum resolution achievable by over-sampling is limited by the temporal spread of the ions produced in each modulation pulse. Examination of Table 1 makes this fact apparent. Compare what is found for a 13-bit sequence with a 40 ns modulation bin width and no over-sampling to that with the same modulation bin width but with a 20 ns over-sampling. Figure 6 also shows that reducing the modulation bin width, while keeping the number of passes constant, increases the resolution but simultaneously reduces the sensitivity. The explanation of this behavior is that fewer ions are injected in every modulation pulse.

In contrast to conventional time-of-flight where the highest achievable temporal resolution is limited by the temporal response of the detector and the sharpness of the temporal definition of the start time, the temporal resolution in HT-TOFMS (for ideal modulation) is limited by the maximum operating frequency of the clock used to generate the sequence. In our implementation of the pseudo-random sequence generation the maximum frequency achievable is 50 MHz, that is, a modulation bin width of 20 ns. The maximum possible time spread between ions at this modulation frequency is therefore 20 ns. In the case of reserpine, which has a flight time of 130 μs, this time spread would result in a theoretical maximum mass resolution ($m/\Delta m$) of 3275. In practice, this resolution has not yet been achieved because modulation bin widths lower than 40 ns increase the switching noise of the push-pull amplifier connected to the

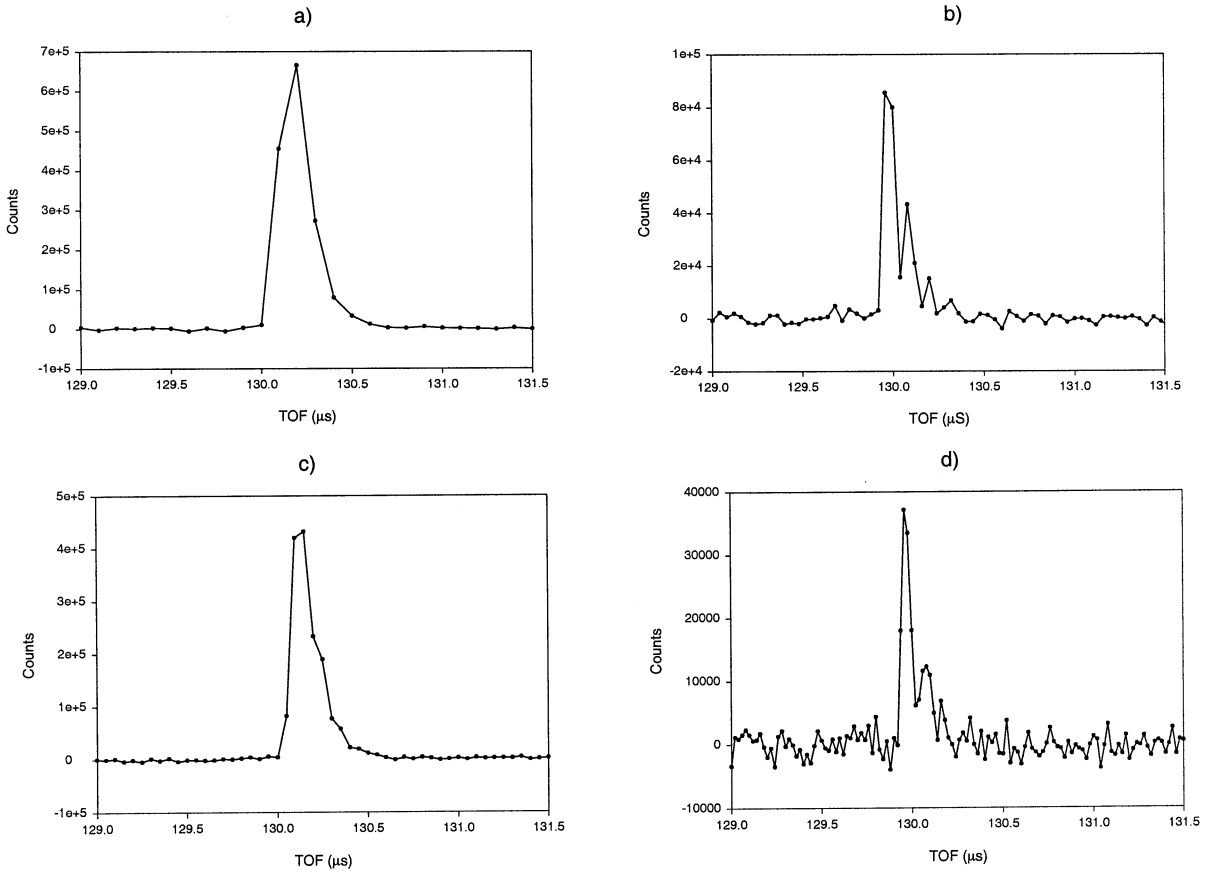

Figure 6. Effect of the modulation and acquisition time bins on the resolution under a 12 bit pseudo-random sequence. (**a**) 100 ns modulation bin, 100 ns acquisition bin; (**b**) 40 ns modulation bin, 40 ns acquisition bin; (**c**) 100 ns modulation bin, 50 ns acquisition bin; and (**d**) 40 ns modulation bin, 20 ns acquisition bin. (50,000 passes).

modulator. Improvements in the shielding of our components should limit the radio frequency noise in the spectrum. The use of faster modulations is also limited, however, by the signal ringing and distorted pulse shapes produced each time a logical 1 is applied to the modulation grid. Future modifications to the electronics, such as high speed diode clamping, improved impedance matching, and the use of broader band amplifiers are expected to permit modulations at faster rates.

Another interesting aspect of our system is the mass cutoff that is created by the modulation process. This cutoff effect is related to the speed of the ions in the proximity of the grid where the modulated field is operational. Given the synchronization requirements of our experiment, it seems clear that only ions that are correctly modulated will contribute to the signal. Improper modulation of ions traveling slowly enough to experience both on and off pulses in the effective modulation region will harm the integrity of the detected signal. The incorrectly modulated ions will contribute to the average background noise because they arrive at times not correlated with the pulsing sequence. For a beam energy of 1250 eV, the theoretical mass cutoff is approximately 12,000 aμ [18]. The working mass range given in Table 1 is set either by the mass cutoff calculated with this expression or by the maximum flight time allowed by the period $N{\cdot}\Delta t$ of a given pseudo-random sequence. Taking into account the normal mass range in ESI, it seems clear that a 13-bit pseudo-random sequence with 40 ns modulation bins width should provide an excellent compromise between useful mass range (almost 4000 aμ), scan speed (3000 Hz) and resolution (1200). For experiments not demanding high mass range, switching to a 12-bit sequence while keeping the same bin widths will increase the scan speed to 6000 Hz with an excellent resolution for most of the analytical applications currently performed. In this study we have shown how the choice of the length of the pseudo-random sequence of 1's and 0's affects the mass range, scan speed, and mass resolution so that the experimenter can choose conditions most appropriate to a particular mass analysis.

Acknowledgments

The authors thank Dr. A. Brock for his invaluable expertise and helpful advice. FMF thanks Fundación Antorchas, Fundación Ciencias Exactas y Naturales, and the FOMEC postdoctoral program for financial support. JMV thanks the Fullbright Commis-

sion for his postdoctoral fellowship. MW thanks the Wallenberg Foundation and Uppsala University for financial support.

References

1. Cotter, R. J. *Time-of-flight Mass Spectrometry*, Washington, DC: ACS Symposium Series No. 549, 1994.
2. Karas, M.; Bachmann, D.; Hillenkamp, F. *Anal. Chem.* **1985,** *57,* 2935–2939.
3. Zenobi, R.; Knochenmuss, R. *Mass Spectrom. Rev.* **1999,** *17,* 337–366.
4. Chien, B. M.; Michael, S. M.; Lubman, D. *Int. J. Mass Spectrom.* **1994,** *131,* 149–179.
5. Guilhaus, M.; Selby, D.; Mlynski, V. *Mass Spectrom. Rev.* **2000,** *19*, 65–107.
6. Brock, A.; Rodriguez, N.; Zare, R. N. *Anal. Chem.* **1998,** *70,* 3735–3741.
7. Brock, A.; Rodriguez, N.; Zare, R. N. *Rev. Sci. Instrum.* **2000,** *71,* 1306–1318.
8. Harwit, M. D.; Sloane, N. J. *Hadamard Transform Optics.* Academic Press: London, 1979, pp 214–216.
9. Marshall, A. G. *Fourier, Hadamard, and Hilbert Transforms in Chemistry.* Plenum Press: New York, 1982, pp 45–67.
10. Treado, P. J.; Morris, M. D. *Spectrochim. Acta Rev.* **1990,** *13,* 355–375.
11. Treado, P. J.; Morris, M. D. *Anal. Chem.* **1989,** *61,* 723A–734A.
12. Barnidge, D. R.; Nilsson, S.; Markides, K. E.; Rapp, H.; Hjort, K. *Rapid Comm. Mass Spectrom.* **1999,** *13,* 994–1002.
13. Ervin, K. M.; Armentrout, P. B. *J. Chem. Phys.* **1985,** *83,* 166–189.
14. Krutchinsky, A. N.; Chernushevich, I. V.; Spicer, V. L.; Ens, W.; Standing, K. G. *J. Am. Soc. Mass Spectrom.* **1998,** *9,* 569–579.
15. Vlasak, P. R.; Beussman, D. J.; Davenport, M. R.; Enke, C. G. *Rev. Sci. Instrum.* **1996,** *67,* 68–72.
16. Montgomery, D. C. *Design and Analysis of Experiments; 4th ed.* Wiley: New York, 2001, pp 466–472.
17. Wilhelmi, G.; Gompf, F. *Nucl. Instr. Meth.* **1970,** *81,* 36–44.
18. Rodriguez, N. Ph.D. Dissertation, Department of Chemistry. Stanford University, 1999.
19. Hanley, Q. S. *Appl. Spectrosc.* **2001,** *55,* 318–330.
20. Koleske, D. D.; Sibener, S. J. *Rev. Sci. Instrum.* **1992,** *63,* 3852–3855.